



## Novel sinuous band microelectrode array for electrochemical amperometric sensing

Yang Li<sup>a</sup>, Shuqing Yin<sup>a</sup>, Nan Jiang<sup>a</sup>, Xinxin Li<sup>a</sup>, Chong Liu<sup>a,b,\*</sup>, Jingmin Li<sup>a,\*</sup>, Yuanchang Liu<sup>c</sup>

<sup>a</sup> Key Laboratory for Micro/Nano Technology and System of Liaoning Province, Dalian University of Technology, Dalian, China

<sup>b</sup> Key Laboratory for Precision and Non-traditional Machining Technology of Ministry of Education, Dalian University of Technology, Dalian, China

<sup>c</sup> Department of Mechanical Engineering, University College London, Torrington Place, WC1E 7JE London, UK

### ARTICLE INFO

#### Keywords:

Amperometric  
Tilt  
Bend  
Sinuous band microelectrode

### ABSTRACT

Pursuing a higher response signal is the core challenge in improving the detection performance of a microelectrode-based amperometric electrochemical sensor. Band microelectrode arrays (bMEAs) are attractive due to their high response current and economical fabrication process. However, further amplifying the response current by arranging the array more compactly or increasing its size is generally hindered by the shielding effect or the restricted construction region. A novel array of sinuous band microelectrodes (sbMEA) is proposed, produced by deforming a bMEA by tilting and bending. Its response and diffusion characteristics are simulated and analyzed. The effects of structural parameters on its performance are revealed, and their optimal value is deduced. The simulation demonstrates that a sbMEA can generate a larger current than a MEA of traditional shape. Production of such a sbMEA does not involve any additional fabrication costs compared with a bMEA. Cyclic voltammetry (CV) tests with potassium ferrocyanide solution verify the theoretical performance of the sbMEA, and a 10% higher current was obtained compared to the corresponding bMEA.

### 1. Introduction

Microelectrode-based electrochemical sensors integrated with microfluidic chips have attracted attention as a promising platform for applications such as disease diagnosis and environmental monitoring in resource-limited non-laboratory conditions [1–4]. Amperometric sensors are the most popular and common type [5], and amplifying the response current is the core challenge for detecting an analyte in trace amounts [6]. Conventionally, numerous microelectrodes are applied simultaneously as an array (MEA) to obtain a measurable response current and reduce interference [7–10]. The response of each microelectrode is determined by its size and shape. Comparing microelectrodes of different shapes, band microelectrode arrays (bMEAs) are often the preferred choice [11–13]. The microscopic width of a single electrode helps to increase the response current density by enhancing the mass diffusion efficiency [14,15], while its macroscopic length is conducive to enlarging its surface area in order to generate a higher response current [16,17]. In addition, bMEAs are thin two-dimensional structures, and can be produced economically by microfabrication techniques [18–20].

To maximize the response current of bMEAs, more electrodes should

be arranged in the restricted construction region by narrowing the interstices as far as possible. The minimized interstices should be twice the thickness of the efficient diffusion layer [21]; if the interstices are too narrow this will lead to an attenuation in the response current due to the overlap and interference of the diffusion field between adjacent electrodes (known as the shielding effect) [22,23]. Although increasing the width of each electrode could amplify the response, this is inadvisable as it will decrease the current density and signal-to-noise ratio [24]. Therefore, designing a new microelectrode with a distinctive shape may be the solution to pushing these limitations, but hardly any research on this topic has been reported in recent decades. A sinuous band microelectrode array (sbMEA) is proposed. This is a deformation of a bMEA by tilting and repeated bending in the plane parallel to the substrate. The effects of structural parameters on the performance of the sbMEA are analyzed with a 3D simulation model. The response current of each electrode is amplified owing to the enlarged surface area. The emerging convex and concave corners change the character of the diffusion distribution; thus, the sinuous band microelectrode array (sbMEA) can be arranged more compactly to yield a higher response current. Due to its thin 2D structure, using a sbMEA does not require any additional fabrication or expense compared with a bMEA of similar size. The

\* Corresponding authors at: Dalian University of Technology, No.2 Linggong Road, Ganjingzi District, Dalian City, Liaoning Province, China.

E-mail addresses: [chongli@dlut.edu.cn](mailto:chongli@dlut.edu.cn) (C. Liu), [jingmin@dlut.edu.cn](mailto:jingmin@dlut.edu.cn) (J. Li).

<https://doi.org/10.1016/j.elecom.2021.107159>

Received 13 October 2021; Received in revised form 30 October 2021; Accepted 30 October 2021

Available online 1 November 2021

1388-2481/© 2021 The Authors.

Published by Elsevier B.V. This is an open access article under the CC BY-NC-ND license

(<http://creativecommons.org/licenses/by-nc-nd/4.0/>).

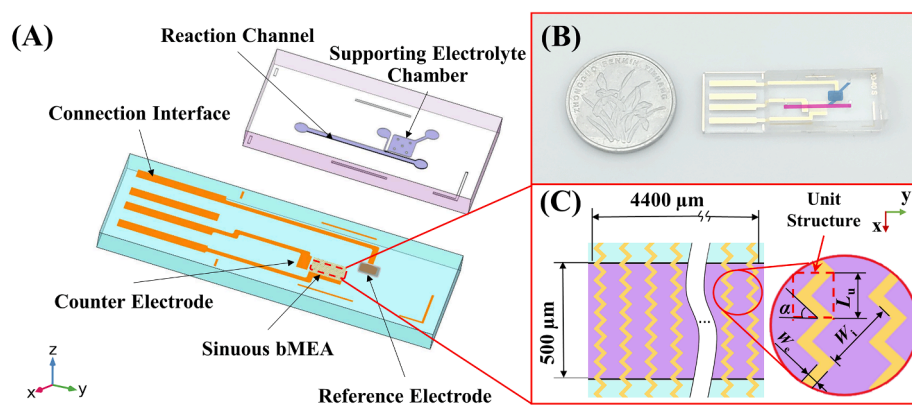


Fig. 1. The structure of the microfluidic chip. (A) Exploded view; (B) assembled chip; and (C) details of the sbMEA.

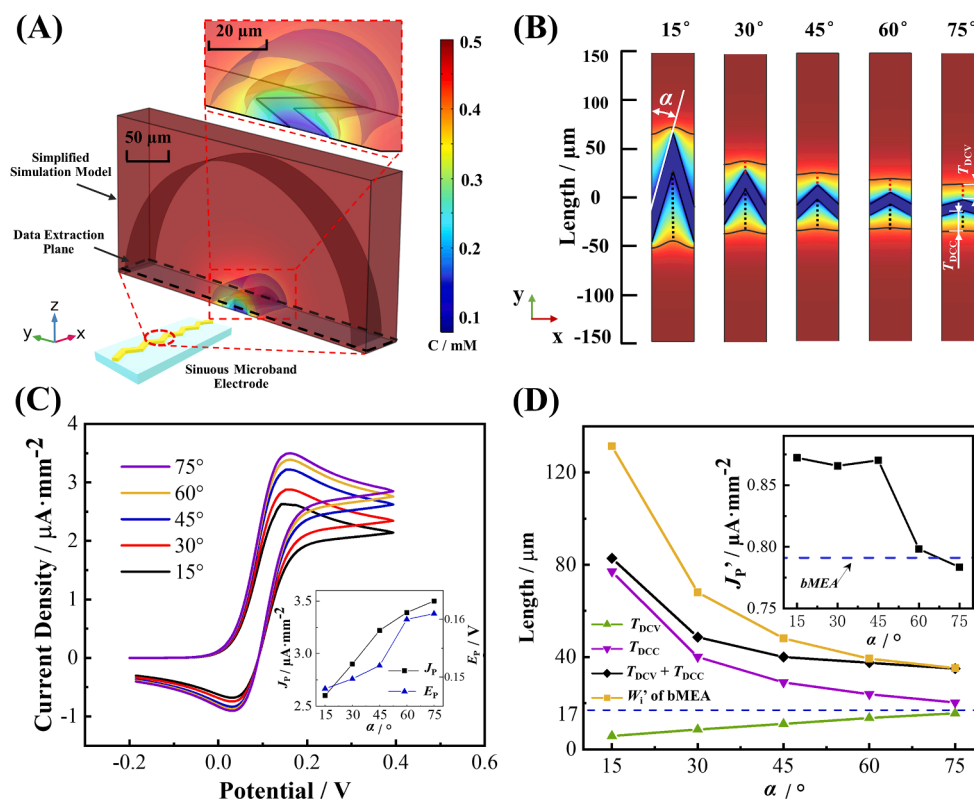


Fig. 2. Simulation results for sbMEA with different slope angles ( $\alpha$ ). (A) Simplified simulation model of the sbME; (B) diffusion field variation; (C) simulated CV voltammograms, inset: plots of  $J_p$  and  $E_p$  vs  $\alpha$ ; and (D) thickness of the efficient diffusion layer at convex corners ( $T_{DCV}$ ) and concave corners ( $T_{DC}$ ), their sum, and the projection of the interstices of a bMEA on the tilting direction ( $W'$ ), inset: the curve of the equivalent current density of a sbMEA.

amplification performance of a sbMEA is verified using cyclic voltammetry (CV) with potassium ferrocyanide solution.

## 2. Experimental

### 2.1. Materials and instrumentation

Details of the chemical reagents and instruments used are given in the [Supplementary Information](#).

### 2.2. Fabrication of a sbMEA integrated within a microfluidic chip

The structures of the sbMEA and microfluidic chip are shown in [Fig. 1\(A\)](#); they are produced using a microfabrication process. Compared

to the corresponding bMEA, the structure in the depth direction is unaltered, and the deformation only occurs in the  $x - y$  plane, which does not increase complexity or cost in manufacturing. The sbMEA is fabricated on a Pyrex glass substrate coated with titanium (50 nm) and gold (150 nm). The sbMEA is patterned using a typical lithography and wet etching process, and its effective construction region is  $4400 \mu\text{m} \times 500 \mu\text{m}$  in the reaction channel. A counter electrode (CE) and a reference electrode (RE), both  $1500 \mu\text{m} \times 1900 \mu\text{m}$  in size, are fabricated by the same method. The RE is further coated with Ag/AgCl. The connection interface is attached to a standard USB plug. A PDMS (polydimethylsiloxane) cover plate containing microchannels is fabricated by pouring using a mold formed with a SU-8 photoresist. The cover plate is bound to the sbMEA by oxygen plasma treatment. In the assembled chip, shown in [Fig. 1\(B\)](#), the reaction channel for the injection of analyte

solution and the supporting electrolyte chamber are colored red and blue, respectively. The chamber is filled with 3 M KCl solution before use in order to stabilize the potential of the RE.

### 2.3. Simulation of a sinuous band microelectrode

A simulation model is constructed to evaluate the performance of a sinuous band microelectrode. In order to analyze the impacts of the structural parameters on the response, the CV voltammogram and the diffusion distribution in the plane of the electrode's upper surface when the oxidation peak occurs (about 3.55 s after the start of the scan) are simulated. Other types of microelectrodes of the same size are also simulated with this model for comparison. As the sinuous band is a complex of multiple symmetric V-type unit structures, as shown in Fig. 1 (C), the 3D simulation model is simplified and constructed as shown in Fig. 2(A) using COMSOL Multiphysics (version 4.3a, Burlington, MA). The model is defined using the width ( $W_e$ ), tilting angle ( $\alpha$ ), and length of the unit ( $L_u$ ). The thickness of the electrode is 200 nm, consistent with the sputter-coated metal layers.  $W_e$  is 10  $\mu\text{m}$  for consistency with the control group while  $\alpha$  and  $L_u$  are variable. The simulation space is defined as 300  $\mu\text{m}$  wide (y direction), 150  $\mu\text{m}$  high (z direction), and  $L_u$  long (x direction); the solution in the space at the initial moment is set as 0.5 mM  $\text{K}_4[\text{Fe}(\text{CN})_6]$  in 0.1 M KCl. To meet the semi-infinite diffusion condition, all the boundaries are set as 'open boundary' except the bottom, and the solution outside these boundaries is the same as at the initial moment. To exclude the charging current, the double-layer capacity of the electrode is ignored. The CV method is applied with a scan rate of 100 mV/s from  $-0.2$  V to 0.4 V. The GMRES (generalized minimum residual) method is employed to solve the simulation model.

The response performance of an array is not determined only by single electrode size but also the width of the minimized interstices ( $W_i$ ). Therefore, the equivalent peak current density of the array ( $J_p'$ , described by Eq. (1)) is introduced as an indicator, where  $I_p$  and  $J_p$  are the peak current and peak current density of a single microelectrode, respectively, and  $W_e'$  and  $W_i'$  equal  $W_e/\sin \alpha$  and  $W_i/\sin \alpha$ , which are the projections in the direction of the y axis.  $W_i$  is determined by the sum of the thicknesses of the diffusion field between adjacent electrodes. The boundary of the efficient diffusion field can be estimated approximately as the isoconcentration line, which is 80% of the initial concentration at this scan rate (as discussed in our previous work [25]), and the validity of this assumption in a sbMEA is verified by simulation as shown in Fig. S2.

$$J_p' = n \cdot I_p / S_A = J_p \cdot W_e' / (W_e' + W_i') \quad (1)$$

### 2.4. Performance verification of sbMEA

The sbMEA in the microfluidic chip is connected with the electrochemical workstation through a homemade USB plug. The reaction channel is injected with the analyte solution (0.5 mM  $\text{K}_4[\text{Fe}(\text{CN})_6]$  in 0.1 M KCl), and emptied and rinsed with deionized water after each test. The CV method is applied with a scan rate of 100 mV/s from  $-0.2$  V to 0.4 V. The response current is calculated as the actual current minus the baseline to ignore the charging current component. Each test is repeated at least six times with three chips.

### 2.5. Statistics

Data are presented as mean  $\pm$  standard deviation (SD). The differences between two means are determined by the two-tailed unpaired Student's *t*-test and  $P < 0.01$  is taken as the level of significance.

## 3. Results and discussion

### 3.1. Influence of the tilting angle ( $\alpha$ )

Five types of sinuous band microelectrodes with different  $\alpha$  values are simulated, with  $W_e = 10 \mu\text{m}$  and  $L_u = 40 \mu\text{m}$  in all cases. As shown in the inset of Fig. 2(A), the isoconcentration surfaces are indicated using different colors, and their shape indicates that the diffusion field is sinusously cylindrical and different from that of the band microelectrode. The diffusion field at convex corners presents as an incomplete hemisphere, and is thinner than in other places. At concave corners, the diffusion field was saddle-shaped, and the distance between the adjacent isoconcentration surfaces was greater than at other positions. Under the effect of the convex and concave corners, each isoconcentration surface varies continuously and is not parallel to the electrode, which indicates uneven and flexural mass transfer. This is also verified by the mass transfer streamlines, as shown in Fig. S1.

With increasing values of  $\alpha$ , the peak oxidation current density ( $J_p$ ) is amplified but is always smaller than that of a normal microband electrode of the same width (3.56  $\mu\text{A}/\text{mm}^2$ , simulated with the same model), as shown in Fig. 2(C), which indicates the attenuation effect of the concave corner. However, tilting leads to a larger surface area, the oxidation current  $I_p$  of a single sinuous band microelectrode is always higher than that of the band microelectrode, and the difference is more remarkable with decreasing values of  $\alpha$ . Meanwhile, the oxidation peak potential ( $E_p$ ) decreases with decreasing values of  $\alpha$ , which indicates faster reactant depletion at the electrode.

The variation in thickness of the diffusion field reflects the mass transfer efficiency; thus, a convex structure contributes to an amplification effect, while a concave structure has the opposite effect. As shown in Fig. 2(B), under the same test conditions, the thickness of the efficient diffusion field at a convex corner ( $T_{\text{DCV}}$ , indicated by a dashed red line) becomes larger, and at a concave corner ( $T_{\text{DCC}}$ , indicated by a dashed black line) becomes smaller, than for a band microelectrode of the same width (17  $\mu\text{m}$ ). Observing the curves of  $T_{\text{DCV}}$  and  $T_{\text{DCC}}$  (Fig. 2D), it can be found that  $T_{\text{DCV}}$  is approximately linear with respect to  $\alpha$ ; furthermore, the decrease in  $T_{\text{DCC}}$  decelerates, especially when  $\alpha$  is greater than  $45^\circ$ . This difference is explained and estimated as shown in Fig. S3, where the projection of the transforming diffusion field in the  $x - y$  plane is indicated by the hatched blue area.

At a convex corner, the diffusion field rotates outward and expands with bending. The new emerging diffusion field is a partial hemisphere (its projection is fan-shaped and indicated by orange shading), which is more efficient than the cylindrical field of the original band and leads to a thinner  $T_{\text{DCV}}$ . The partially hemispherical diffusion field expands linearly with increasing intersection angle, which should be twice the supplementary angle of  $\alpha$ . Therefore,  $T_{\text{DCV}}$  should be linear with respect to  $\alpha$ . At the concave corner, the diffusion field rotates inward and overlaps, which is known as the 'self-shielding effect'. As a result, the mass transfer is trapped, and the thickness  $T_{\text{DCC}}$  increases. In addition, the 'self-shielding effect' develops with decreasing  $\alpha$ , not only in a broader scope but also extending into the inner diffusion layer. If  $\alpha$  is smaller than  $45^\circ$ , the partial diffusion field would be shielded by the electrode, and the mass transfer would be entirely cut off in this excessively shielded zone, which explains the dramatic variation in  $T_{\text{DCC}}$  when  $\alpha$  is smaller than  $45^\circ$ .

The performance of sbMEAs with different values of  $\alpha$  is further evaluated in terms of their equivalent peak current density ( $J_p'$ ), as shown in the inset of Fig. 2(D). The  $W_i'$  of a sbMEA is estimated as the sum of  $T_{\text{DCV}}$  and  $T_{\text{DCC}}$ . It should be noted that  $W_i'$  is the projection of  $W_i$  along the y axis rather than perpendicular to the surface. To compare the relative compactness, the  $W_i$  of a bMEA was converted into projection form. The  $W_i'$  of a sbMEA is always smaller than that of a similar bMEA, which indicates that the sbMEA can be arranged more compactly. Thus, it is possible to achieve an amplified  $J_p'$  by using a sbMEA, even though the current density of an individual sinuous band is always smaller than

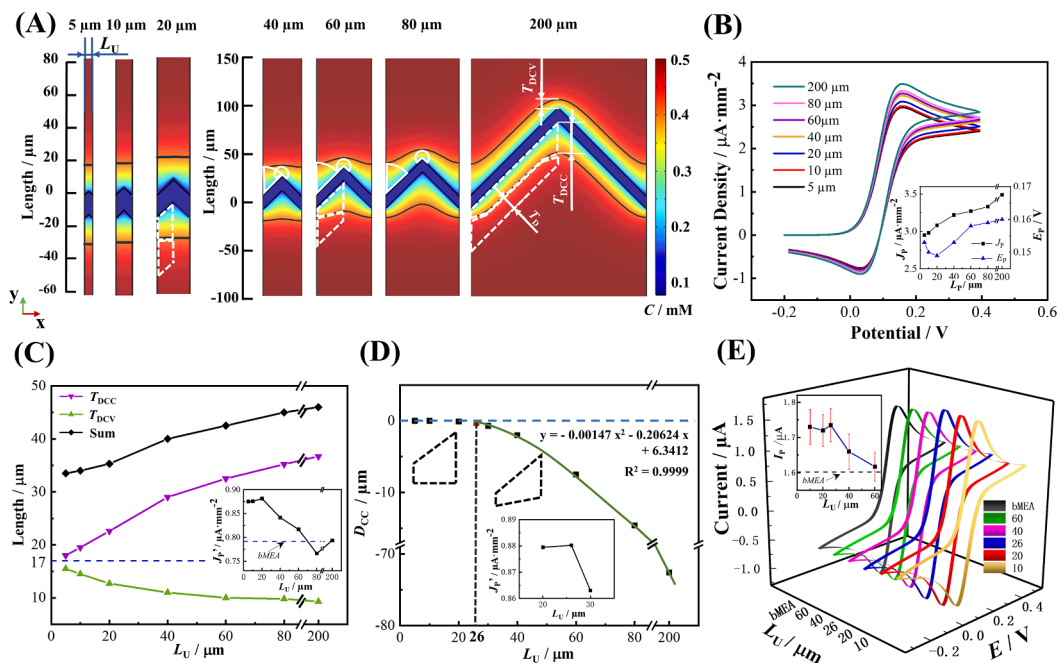


**Fig. 3.** Simulation and experimental results for a sbMEA with different lengths of the unit structure ( $L_u$ ). (A) Variation in the diffusion field; (B) simulated CV voltammograms, inset: the  $J_p$  and  $E_p$  curves; (C) the thickness of the efficient diffusion layer at the convex corner ( $T_{DCV}$ ) and concave corner ( $T_{DCC}$ ), and their sum. Inset: the equivalent current density ( $J_p'$ ) of the sbMEA; (D) the difference in position between the points on the efficient diffusion boundary corresponding to the convex and concave corners ( $D_{cc}$ ) and the quadratic fitting curve. Inset: the curve of  $J_p'$  of the sbMEA; (E) the experimental CV results. Inset: the curve of  $I_p$ , the error bars correspond to the standard deviation ( $n = 5$ ).

that of a normal band. The  $J_p'$  of the sbMEA decreases with  $\alpha$  and becomes smaller than that of a bMEA when  $\alpha$  is greater than  $60^\circ$ . As the attenuation of  $J_p'$  is not significant when  $\alpha$  is smaller than  $45^\circ$ , the optimal  $\alpha$  is taken to be  $45^\circ$ , as a reasonable compromise between increasing  $J_p$  and decreasing  $J_p'$ .

### 3.2. Influence of the length of the unit structure ( $L_u$ )

A group of simplified sinuous band microelectrodes with different values of  $L_u$  is simulated, taking  $W_e = 10 \mu\text{m}$  and  $\alpha = 45^\circ$ . The variation in the diffusion distribution and the  $T_{DCV}$  and  $T_{DCC}$  curves are shown in Fig. 3(A) and (C). The diffusion field is symmetrical and could be considered as an assembly of trapezoidal diffusion units, whose upper base and bottom are  $T_{DCV}$  and  $T_{DCC}$ , respectively. The morphology of the trapezoid varies with  $L_u$ . When  $L_u$  is smaller than  $20 \mu\text{m}$ , the trapezoid is right-angled, and its outer boundary is parallel to the  $x$  axis, which should be a cylindrical surface in space. When  $L_u$  is longer than  $40 \mu\text{m}$ , the trapezoid becomes oblique, and its outer boundary is no longer parallel to the  $x$  axis. The variation in  $T_{DCV}$  and  $T_{DCC}$  could be explained by the overlap of diffusion fields corresponding to convex and concave corners. The scope of the diffusion influence of the convex and concave corners is indicated by auxiliary lines, which are arcs with a radius of  $T_{DCV}$  and  $T_{DCC}$ , respectively (white lines in Fig. 3A). The arcs gradually move apart with increasing  $L_u$ . As a result, the arc corresponding to the convex corner emerges from the overlap, and the mass transfer in this region becomes more efficient, which explains the continuous decrease in  $T_{DCV}$ . The gradual increases in  $J_p$  and  $E_p$  of the CV voltammograms with  $L_u$ , as shown in Fig. 3(B), also support this analysis. The arcs are nearly tangential when  $L_u$  is  $60 \mu\text{m}$ . Thus, the deceleration of  $T_{DCV}$  becomes negligible as  $L_u$  becomes larger, which demonstrates that the distance between the corners is great enough to avoid overlap of the efficient diffusion fields. Thus, the acceleration of  $E_p$  and  $J_p$  becomes slower. The  $J_p$  of a single sinuous band reaches its maximum value when  $L_u$  is very long ( $200 \mu\text{m}$ ); however, it is still lower than that of the band microelectrode. Nevertheless,  $T_{DCC}$  becomes thicker with  $L_u$ . This is

because the diffusion field corresponding to the concave corner not only overlaps with the convex corner but is also affected by the straight part of the electrode, and the overlap region increases with  $L_u$ .

It was surprising that  $E_p$  did not increase monotonically but decreased when  $L_u$  was less than  $20 \mu\text{m}$ , as shown in Fig. 3(B). Observing the diffusion field, we find that the trapezoidal diffusion unit is always right-angled, which indicates that the diffusion distribution and response of the sinuous band should be similar to that of a little wider band, and the equivalent width of the band should be proportional to  $L_u$ . The reactant would be depleted more quickly at a wider electrode, leading to a decrease in  $E_p$ .

To calculate the value of  $J_p'$  for the sbMEA, the minimized interstices of the sbMEA were estimated by splicing the trapezoidal diffusion units belonging to adjacent electrodes, and  $W_i'$  should be the sum of  $T_{DCV}$  and  $T_{DCC}$ . Meanwhile, when  $L_u$  is longer than  $80 \mu\text{m}$ , the diffusion unit part is an irregular hexagon (as shown in Fig. 3(A)).  $W_i'$  is no longer equal to the sum of  $T_{DCV}$  and  $T_{DCC}$ , but is approximately equal to  $2 \cdot T_D / \sin 45^\circ$ , because the thickness of the efficient diffusion field at the straight part becomes similar to that of the band electrode. The variation in  $J_p'$  is shown in the inset of Fig. 3(C). The maximum  $J_p'$  appears when  $L_u$  is about  $20 \mu\text{m}$ . It is speculated that the precise maximum point of  $J_p'$  might be associated with the critical point where the diffusion unit transforms from right-angled to oblique. The shape could be quantitatively evaluated using  $D_{cc}$  (the difference in position between the points on the diffusion boundary corresponding to the convex and concave corners), which is calculated as  $(T_{DCC} - T_{DCV} - L_u/2)$ . The trapezoidal unit should be right angled when  $D_{cc}$  is zero. As shown in Fig. 3(D), the non-zero points are fitted as a quadratic polynomial ( $R^2 = 0.9999$ ), and the critical point of transformation is the point of intersection with the zero line ( $L_u = 26 \mu\text{m}$ ). The additional simulation results in the inset of Fig. 3(D) validate the assumption, and the sbMEA with the estimated optimal  $L_u$  does indeed generate the maximum  $J_p'$ . It should be noted that the optimal value of  $L_u$  is not constant and can be influenced by the analyte solution system, the test parameters, or environmental factors.

**Table 1**  
Performance comparison of MEAs with different shapes.

Shape	$I_p$ / nA *	Minimized interstices / $\mu\text{m}$	$J_p'$ / $\mu\text{A}\cdot\text{mm}^{-2}$
Band	17.9	34	0.813
Cylinder	23.7	44	0.878
Sinuous band	22.1	25.5** / 36	0.881
Disc	0.691	18	0.838
Sphere	1.11	26	0.799

\* The peak oxidation current of a single electrode; \*\* the interstices perpendicular to the electrode.

### 3.3. Performance comparison and verification

Different types of microelectrode of the same size are simulated using the model described above, and the results are given in Table 1. Using a sinuous band instead of the original band elevates the value of  $I_p$  for every individual electrode without changing the feature size. Though the  $I_p$  of a single cylinder is a little higher, the sbMEA can be arranged more compactly due to the narrower minimized interstices, which contributes to a higher total current. Within the same construction region, the sbMEA can generate a higher total response current than a MEA of a traditional shape, as it has the highest value of  $J_p'$ . In addition, the fabrication of the sbMEA does not involve any additional processing or increase in cost, because of its 2-dimensional structure.

Fig. 3(E) shows the experimental CV results for a sbMEA. It can be seen that the optimized structure did indeed produce the maximum oxidation current, which is about 10% higher than that of a comparable bMEA (same width and construction region).

## 4. Conclusion

A novel sinuous band microelectrode array was proposed to amplify the response current in electrochemical sensing. The effects of its unique shape on the response performance and the diffusion field were analyzed and validated by simulation, and its optimal structure was deduced. The simulation results of microelectrodes with different shapes demonstrated that the sbMEA could generate a higher current within the same construction region and test parameters. The experiments showed that using a sbMEA could achieve 10% amplification of the current compared to a bMEA; in addition, the fabrication process and cost would not be affected due to the unchanged width and simple structure in the depth direction.

## 5. Funding information

This work is supported by the National Key R&D Program of China (2020YFB2009002), the National Natural Science Foundation of China (51875084), and the Fundamental Research Funds for the Central Universities (DUT20ZD103).

### CRediT authorship contribution statement

**Yang Li:** Conceptualization, Methodology, Software, Formal analysis, Investigation, Data curation, Visualization, Writing – original draft, Writing – review & editing. **Shuqing Yin:** Investigation, Resources, Validation. **Nan Jiang:** Investigation, Resources. **Xinxin Li:** Software. **Chong Liu:** Conceptualization, Project administration, Supervision, Funding acquisition, Writing – review & editing. **Jingmin Li:**

Conceptualization, Project administration, Supervision, Funding acquisition, Writing – review & editing. **Yuanchang Liu:** Validation, Writing – review & editing.

## Declaration of Competing Interest

The authors declare that they have no known competing financial interests or personal relationships that could have appeared to influence the work reported in this paper.

## Appendix A. Supplementary data

Supplementary data to this article can be found online at <https://doi.org/10.1016/j.elecom.2021.107159>.

## References

- [1] V.S.P.K. Jayanthi, A.B. Das, U. Saxena, *Biosens. Bioelectron.* 91 (2017) 15–23, <https://doi.org/10.1016/j.bios.2016.12.014>.
- [2] J. Wang, *Biosens. Bioelectron.* 21 (2006) 1887–1892, <https://doi.org/10.1016/j.bios.2005.10.027>.
- [3] F. Li, M. You, S. Li, J. Hu, C. Liu, Y. Gong, H. Yang, F. Xu, *Biotechnol. Adv.* 39 (2020), 107442, <https://doi.org/10.1016/j.biotechadv.2019.107442>.
- [4] R.P. Shukla, C. Rapiere, M. Glassman, F. Liu, D.L. Kelly, H. Ben-Yoav, *Electrochem. Commun.* 120 (2020), 106850, <https://doi.org/10.1016/j.elecom.2020.106850>.
- [5] K.K. Mistry, K. Layek, A. Mahapatra, C. Roychoudhuri, H. Saha, *Analyst* 139 (2014) 2289–2311, <https://doi.org/10.1039/c3an02050a>.
- [6] W. Wen, X. Yan, C. Zhu, D. Du, Y. Lin, *Anal. Chem.* 89 (2016) 138–156, <https://doi.org/10.1021/acs.analchem.6b04281>.
- [7] D. Li, C. Batchelor-McAuley, L. Chen, R.G. Compton, *ACS Sensors* 4 (2019) 2250–2266, <https://doi.org/10.1021/acssensors.9b01172>.
- [8] L. Duan, X. Lv, Q. He, X. Ji, M. Sun, Y. Yang, Z. Ji, Y. Xie, *Biosens. Bioelectron.* 150 (2020), 111886, <https://doi.org/10.1016/j.bios.2019.111886>.
- [9] I. Shitanda, Y. Fujimura, S. Nohara, Y. Hoshi, M. Itagaki, S. Tsujimura, *J. Electrochem. Soc.* 166 (2019) B1063–B1068, <https://doi.org/10.1149/2.1501912jes>.
- [10] M.Y. Vagin, A.N. Sekretaryova, R.S. Reategui, I. Lundstrom, F. Winquist, M. Eriksson, *Chemelectrochem* 1 (2014) 755–762, <https://doi.org/10.1002/celec.201300204>.
- [11] M. Al Khatib, M. Bellini, R. Pogni, A. Giaccherini, M. Innocenti, F. Vizza, A. Lavacchi, *Sensors* 18 (2018) 3196, <https://doi.org/10.3390/s18103196>.
- [12] H. Ohnuki, T. Wako, B. Mecheri, H. Wu, D. Tsuya, H. Endo, *SBBG16, Jpn. J. Appl. Phys.* 58 (2019), <https://doi.org/10.7567/1347-4065/ab01d2>.
- [13] S. Ko, B. Kim, S. Jo, S.Y. Oh, J. Park, *Biosens. Bioelectron.* 23 (2007) 51–59, <https://doi.org/10.1016/j.bios.2007.03.013>.
- [14] S. Eloul, E. Kätelhön, C. Batchelor-McAuley, K. Tschulik, R.G. Compton, *J. Electroanal. Chem.* 755 (2015) 136–142, <https://doi.org/10.1016/j.jelechem.2015.07.042>.
- [15] R. Usha Rani, L. Rajendran, *Electrochemistry Communications* 128 107071 (2021), <https://doi.org/10.1016/j.elecom.2021.107071>.
- [16] H. Le, R.G. Compton, *J. Electroanal. Chem.* 866 (2020), 114149, <https://doi.org/10.1016/j.jelechem.2020.114149>.
- [17] T. Adachi, Y. Kitazumi, O. Shirai, K. Kano, *Sensors* 20 (2020) 4826, <https://doi.org/10.3390/s20174826>.
- [18] M. Li, W.H. Li, J. Zhang, G. Alici, W. Wen, *J. Phys. D Appl. Phys.* 47 (2014) 63001, <https://doi.org/10.1088/0022-3727/47/6/063001>.
- [19] M. Samuelsson, M. Armgarth, C. Nylander, *Analytical Chemistry* (Washington) 63 (1991) 931–936, <https://doi.org/10.1021/ac00009a020>.
- [20] L. Syedmoradi, M. Daneshpour, M. Alvandipour, F.A. Gomez, H. Hajghassem, K. Omidfar, *Biosens. Bioelectron.* 87 (2017) 373–387, <https://doi.org/10.1016/j.bios.2016.08.084>.
- [21] C. Belmont, M.L. Tercier, J. Buffle, G.C. Fiaccabrino, M. Koudelka-Hep, *Anal. Chim. Acta* 329 (1996) 203–214, [https://doi.org/10.1016/0003-2670\(96\)00116-X](https://doi.org/10.1016/0003-2670(96)00116-X).
- [22] P. Tomčík, *Sensors* 13 (2013) 13659–13684, <https://doi.org/10.3390/s131013659>.
- [23] X. Xie, D. Stüben, Z. Berner, J. Albers, R. Hintsche, E. Jantzen, *Sens. Actuators, B* 97 (2004) 168–173, <https://doi.org/10.1016/j.snb.2003.08.012>.
- [24] J. Min, A.J. Baeumner, *Electroanalysis* 16 (2004) 724–729, <https://doi.org/10.1002/elan.200302872>.
- [25] Y. Li, S. Zuo, L. Ding, P. Xu, K. Wang, Y. Liu, J. Li, C. Liu, *Anal. Bioanal. Chem.* 412 (2020) 8325–8338, <https://doi.org/10.1007/s00216-020-02968-z>.